IEEE Access
Multidisciplinary ⋮ Rapid Review ⋮ Open Access Journal

Received 1 December 2023, accepted 25 December 2023, date of publication 2 January 2024,
date of current version 11 January 2024.

*Digital Object Identifier 10.1109/ACCESS.2023.3349149*

RESEARCH ARTICLE

# High-Resolution Bathymetry by Deep-Learning Based Point Cloud Upsampling

**NAOYA IRISAWA[1,2] AND MASAAKI IIYAMA[1], (Member, IEEE)**
[1]Graduate School of Data Science, Shiga University, Hikone, Shiga 522-8522, Japan
[2]Ecomott Inc., Sapporo, Hokkaido 060-0031, Japan

Corresponding author: Naoya Irisawa (irisawanaoya.ds@gmail.com)

This work was supported in part by the Japan Science and Technology Agency (JST), Core Research for Evolutional Science and Technology (CREST), under Grant JPMJCR19F1; and in part by the Japan Society for the Promotion of Science (JSPS) KAKENHI, Japan, under Grant 21H04913.

**ABSTRACT** Gridded bathymetric data are often used to understand seafloor topography; however, high-resolution data are rare. To obtain high-resolution gridded bathymetric data, the observations from which the data are derived must be densely measured. However, this process is time consuming and expensive. In this study, we propose a method to obtain dense bathymetric data from sparse observations by treating the observed data as a 3D point cloud and applying a deep-learning-based point cloud upsampling technique. The upsampled cloud points were converted into gridded form. The effectiveness of our method was verified through both quantitative and qualitative analyses.

**INDEX TERMS** Bathymetry, deep learning, point clouds, super-resolution.

## I. INTRODUCTION

Understanding detailed seafloor topography is important for various applications, including the protection of marine resources and construction of infrastructure.

Bathymetric data can be obtained using shipborne, airborne, and satellite-based methods. Shipborne measurements are the primary approach for collecting large-scale bathymetric data. Two systems were used for the shipborne measurements: multibeam sonar and single-beam sonar systems. Both systems capture seafloor topology as point clouds, which are then transformed into gridded data for practical use. To obtain high-quality bathymetric data, various methods have been studied to obtain high-quality bathymetric data by considering topographic information, instrument characteristics, and effects of the measurement environment [1], [2].

However, according to the Seabed 2030 project [3], only 23.4% of the total seafloor has been mapped using gridded bathymetric data. The major reason for this is the cost of data acquisition. To map the seafloor topography using single-beam sonar, which measures the topography below the ship, continuous measurements are required as the ship moves forward. These measurements were taken at closely spaced intervals to ensure thorough coverage in the ship's wake. By contrast, multibeam sonar extends its capabilities beyond the area below the ship to include the surrounding topography, allowing for a less dense wake interval. However, a multibeam sonar system is more expensive than a single-beam sonar. In addition, despite its wider range, multibeam sonar requires a relatively short wake interval for detailed topographic measurements.

To address this problem, machine-learning super-resolution techniques have been proposed [4], [5]. These techniques treat gridded bathymetric data as images and apply image super-resolution techniques. High-resolution gridded bathymetric maps can be obtained from existing low-resolution gridded bathymetric maps. However, the information that remained in the original point cloud data, but not in the gridded data, was not used. When converting point clouds into gridded data via Kriging [6] which is an interpolation method, variability exists in the number of corresponding point clouds for each grid cell. Several cells may contain numerous point clouds, while others may not. This variability is particularly evident when there is a large interval in the wake of the ship. Traditional super-resolution

The associate editor coordinating the review of this manuscript and approving it for publication was Gerardo Di Martino.

methods do not adequately address these variations, which subsequently becomes a bottleneck in improving super-resolution performance.

In this study, we propose using direct bathymetric data rather than gridded bathymetric data to improve the accuracy of seafloor topography representations. Specifically, bathymetric data were processed as 3D point cloud structures, and dense bathymetric information was derived from sparse bathymetric data using a deep-learning-based point cloud upsampling technique.

In a practical and cost-conscious scenario, we based our approach on single-beam sonar data. Our model was designed to process topography data collected over wide wake intervals, transforming this input into dense topography data represented as point clouds. These point clouds were then converted into a gridded format to produce high-resolution bathymetric data.

To train our model, we used dense multibeam sonar measurements from publicly available datasets. Using these datasets, we synthesized data that mimicked single-beam sonar measurements. Based on the synthesized data, a neural network capable of reconstructing the original dense measurement data was constructed. Our model can generate dense measurement data for uncharted bathymetric areas that are not included in the datasets.

The main contributions of this study are as follows:

1) To the best of our knowledge, this is the first study to apply a point cloud upsampling technique to bathymetric data.
2) We also propose a method for constructing a dataset from actual bathymetric data so that point cloud upsampling techniques to be applied.
3) From the quantitative and qualitative results, our proposed method can generate more detailed bathymetric data from sparse bathymetric data.

Note that our method does not make any assumptions on instrument characteristics and topographic information. Our method can be combined with existing characteristics-aware bathymetric method and upsample outputs from the existing method

The structure of this paper is as follows. First, we review related work on improving the quality of bathymetric maps and point cloud upsampling techniques. Next, we describe the procedure for generating the bathymetric dataset and the proposed point cloud upsampling method for the bathymetric data. Furthermore, we present the results of the proposed method, including quantitative and qualitative evaluations. Finally, we conclude the paper with a discussion and summary of this study.

## II. RELATED WORK

We briefly review studies on the super-resolution of bathymetric maps, that is, the construction of high-resolution gridded bathymetric data and recent point cloud upsampling techniques.

### A. SUPER-RESOLUTION OF BATHYMETRIC MAPS

Despite the importance of high-resolution bathymetric data in understanding seafloor characteristics, the availability of such data remains limited. Recently, several methods have been developed to generate high-quality bathymetric data [4], [5], [8], [10]. For example, Sonogashira et al. [4] proposed a deep-learning-based super-resolution model for gridded bathymetric data. Their study showed that the ESRGAN model [7], trained on both low- and high-resolution bathymetric maps, had superior accuracy over traditional interpolation techniques such as bilinear interpolation. However, this method requires a substantial gridded bathymetric dataset, which is difficult to obtain because the existing data are both limited and have coarse resolution. Consequently, several studies have attempted to mitigate the scarcity of bathymetric data by applying transfer-learning methods [8], [10]. In particular, Zhang et al. [8] drew attention to the similarities between terrestrial and oceanic landscapes by constructing a pretrained model using land samples. This model, which is based on the EDSR architecture [9], was fine-tuned to accommodate the limited bathymetric data available.

In contrast, the learning process in deep learning is often referred to as a "black box," and notes for its low interpretability. To address this issue, Yutani et al. [5] extended the sparse coding super-resolution technique and proposed a super-resolution method for bathymetric maps that provided high interpretability of the results.

### B. POINT CLOUD UPSAMPLING

A point cloud is a representation of 3D data and is often acquired through geospatial measurements using sensors, such as LiDAR. With the recent advancements in 3D sensor technology, the acquisition of point cloud data has become increasingly accessible. Simultaneously, the emergence of deep learning techniques that automatically extract features has led to superior performance in tasks such as 3D class classification, 3D object detection, and segmentation. However, a distinguishing characteristic of point cloud data, particularly those derived from sensors such as LiDAR, is that they often contain noise or exhibit nonuniformity. This characteristic distinguishes point cloud data from images in which the pixels are arranged in a regular and systematic manner. The nature of point clouds presents challenges and considerations when processing and analyzing them.

Point cloud upsampling, a task aimed at transforming sparse or noisy point clouds into dense or comprehensive forms, has recently emerged as a topic of interest. In particular, deep-learning-based approaches, such as PU-Net [12], which extracts features through hierarchical downsampling and subsequently generates points, have demonstrated remarkable performance. Subsequently, various methods have been proposed [13], [14], [15], [16]. A typical point cloud upsampling model consists of three essential modules: feature extraction, feature upsampling, and point cloud

generation. The training of the model was achieved by minimizing the error of the generated point cloud with the ground truth point cloud.

## III. METHOD

In this study, we present a method for generating dense bathymetric data from sparse bathymetric data. We constructed a dataset derived from real bathymetric data and applied deep learning-based point cloud upsampling techniques to bathymetric data. The key point of this method is that bathymetric data are treated as 3D point cloud data, providing high-quality bathymetric data.

### A. OVERVIEW

An overview of the proposed method is presented in Fig. 1. The proposed method consisted of two parts: dataset construction and model training. The observed data of bathymetry is given as a set of points expressed in 3D coordinates of latitude, longitude, and depth, and the proposed method trains a network with $N$ points as the input and $rN$ points as the output, where $r$ is the upsampling factor. In this study, these are referred to as sparse and dense point clouds, respectively. The dataset construction consisted of two steps. The first is a preprocessing step to remove missing or noisy data from the raw bathymetry, and the second is to construct the sparse and dense point clouds needed to train the network. The latter step generates data that simulate the measurements made by a vessel using a single-beam sonar system.

### B. DATASET AND DATA CLEANSING

For the actual bathymetric data used in this study, we used measurements provided by JAMSTEC,[1] which were acquired using a multibeam sonar system. These data consisted of three dimensions: longitude, latitude, and depth. For this experiment, the ocean region was segmented into 15 arcmin of latitude and longitude, equivalent to approximately 27 000 m, and each sample was transformed into a Cartesian coordinate system with the origin set at (minimum longitude, minimum latitude, 0). The z-axis, which represents the depth, was oriented downward. In addition, we selected samples within the coordinates from (N 20;30;00, E 123;00;00) to (N 45;30;00, E 154;00;00), which includes the sea area around Japan. From the selected samples, we employed a data-cleansing method and subsequently prepared dense and sparse bathymetric data. These datasets were used to train and evaluate the proposed method. Figure 2 presents a visual representation of a sample of the bathymetric data.

The point cloud upsampling model assumes that the object being processed has a single, continuous, smooth surface. However, the samples obtained using this method may contain multiple continuous regions. In Fig. 2, there are two regions in a sample: a large continuous region in the center of the figure and a small region in the upper right corner of the figure. To maintain the model assumptions, the samples must be processed such that each contains only one continuous region. In addition, raw observations may contain data measured multiple times at nearby locations or noise from unremoved observations, both of which must be eliminated. To address these issues, three pre-processing steps were performed for each sample: clustering, removal of redundant observations, and removal of outliers.

#### 1) CLUSTERING

As it is desirable to have only one continuous region in a given sample (15 × 15 arc-minute sea area), we applied a clustering process. Specifically, HDBSCAN [17], which is a density-based clustering method, was applied to the observed points in each sample, and the cluster with the largest number of points was extracted.

#### 2) REMOVAL OBSERVATION POINTS

Due to the raw data collection process, where seafloor topography was observed as the ship moved, there were variations in the distribution of the measurements. Specifically, there are areas where the vessel makes numerous close observations, and conversely, areas where the vessel rarely visits, resulting in a lack of observations. Therefore, we removed these sparse observation points by calculating the distribution (i.e., density) of the points around each point. Specifically, we define the following set:

$$N_\epsilon(\boldsymbol{p}) := \left\{ \boldsymbol{q} \in P_{\text{obs}} \;\middle|\; \|\boldsymbol{p} - \boldsymbol{q}\| \leq \epsilon \right\}, \quad \boldsymbol{p} \in P_{\text{obs}} \subseteq \mathbb{R}^2$$

where $P_{\text{obs}}$ denotes the set of observation points $(x, y)$ in the bathymetric data. In other words, the set $N_\epsilon(\boldsymbol{p})$ is a neighborhood of radius $\epsilon$ centered on observation point $\boldsymbol{p} \in P_{\text{obs}}$. The number of elements in this set is denoted by $k(\boldsymbol{p})$. $k(\boldsymbol{p})$ was calculated for each observation point in each sample, and bathymetric data below the specified number of neighborhood points (minimum neighborhood points) were removed. The maximum number of neighborhood points is also defined to ensure that bathymetric data with an extremely high number of points are removed. In our method, $\epsilon$ was set to 1000 m, and the minimum and maximum numbers of points in the neighborhood were set to 80 and 5000, respectively.

#### 3) OUTLIER REMOVAL

The depth values contain outliers owing to the influence of the measurement environment. In particular, outliers in multibeam bathymetric data are caused by several factors [18]. Because the outlier removal process is time consuming, many methods have been proposed to automatically remove outliers [19], [20]. To apply the outlier removal process to various bathymetric data (different seafloor contexts), we used local information on seafloor topography. Specifically, bathymetric values were estimated using Ordinary Kriging [6] for each point, and bathymetric data in which the absolute error (APE) between the actual and estimated

[1] DARWIN (http://www.godac.jamstec.go.jp/darwin/):bathymetric data

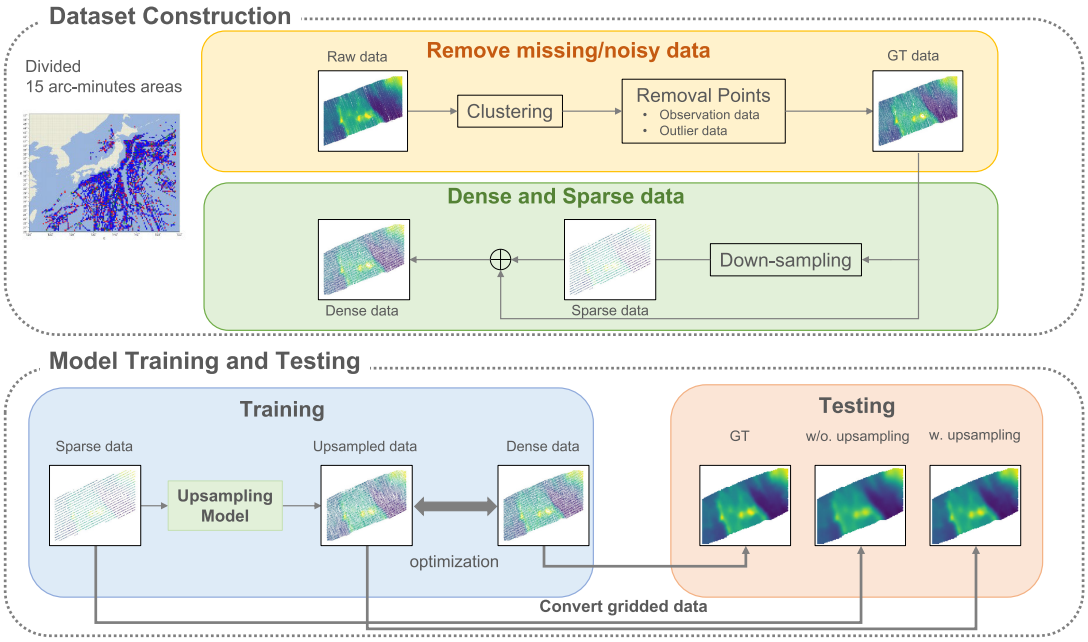


**FIGURE 1.** Overview of our method. First, we construct the dataset for our method from actual bathymetric data. The dataset is a pair of sparse and dense bathymetric data, and we generate the sparse bathymetric dataset by thinning points from the dense bathymetric data. Next, the model learns the generation of dense bathymetric point cloud from sparse bathymetric point cloud. In the testing phase, each point cloud data is converted to gridded data for evaluation of the effect of upsampling.

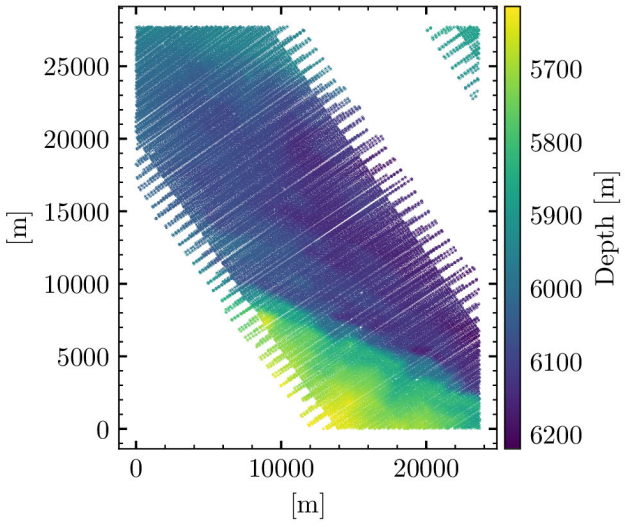


**FIGURE 2.** A sample of bathymetric data. The origin represents (minimum longitude, minimum latitude, 0).

bathymetric values exceeded a certain value were removed. That is, for each observation point $\boldsymbol{p} \in P_{\text{obs}}$, we removed the bathymetric data that satisfied the following equation:

$$\frac{|\bar{z}(\boldsymbol{p}) - z(\boldsymbol{p})|}{\bar{z}(\boldsymbol{p})} \geq threshold$$

where $z(\boldsymbol{p})$ is the actual observed bathymetric value, and $\bar{z}(\boldsymbol{p})$ is the estimated bathymetric value by Ordinary Kriging. The data used for Kriging calculations were the $k$ nearest points of each bathymetric datum. To make the Kriging process more efficient, the bathymetric data to be estimated were those with less than 50% of the elements intersecting each neighborhood, rather than all data. In our method, the values of $k$ and *threshold* were set to 200 and 0.01, respectively.

#### 4) GROUND TRUTH DATASET

To construct the bathymetric ground truth dataset, samples were selected based on the fulfillment of the following conditions: (1) The total number of points within a sample falls within the range of 20 000 to 50 000. (2) The minimum depth is greater than 1000 m and the maximum depth is less than 7000 m. (3) For both the $x$ and $y$ coordinates, the calculation of the maximum and minimum values shows a difference greater than 7000 m. Next, the number of points for each selected sample was standardized to a constant value of 20 000 points obtained using the farthest point sampling method, and the centers of the $x$ and $y$ coordinates were repositioned parallel to the origin.

Therefore, 3571 sea areas with 15 arcmin of latitude and longitude were extracted. From conditions (1) and (2), the $x$ and $y$ components of the sample can assume values from 7000 m to approximately 27 000 m and the $z$ component can assume values ranging from 1000 m to 7000 m.

### C. DATASET FOR TRAINING UPSAMPLING MODEL

The proposed method trains an upsampling model that uses a sparse point cloud of $N$ points as the input and outputs a

dense point cloud of $rN$ points. However, sparse point clouds corresponding to the dense data used in this study did not exist. Therefore, sparse point clouds $P_{\mathrm{LR}} \subseteq \mathbb{R}^{N\times 3}$ were generated from the ground truth bathymetric data. In addition, dense point clouds $P_{\mathrm{HR}} \subseteq \mathbb{R}^{rN\times 3}$ corresponding to sparse point clouds were created. To train the upsampling model, we constructed a training dataset that satisfied the following two conditions:

- Set the number of points in the sparse and dense point clouds to $N$ and $rN$, respectively.
- Generate a sparse point cloud expecting to measure with a vessel equipped with a single-beam sonar.

#### 1) SPARSE BATHYMETRIC DATA

For real-world applications, we assume that the bathymetric data collected by a single-beam sonar system are represented as sparse point clouds. Because a single-beam sonar system focuses on bathymetric topography immediately below the vessel's wake, the data acquired from a single measurement typically lack extensive information about seafloor topography. Consequently, we considered bathymetric data collected from multiple observations using a single-beam sonar system as sparse data and synthesized this sparse dataset from the ground truth data. Specifically, the wake of the vessel for single-beam sonar observations was modeled as a straight and uniformly spaced path.

First, the direction of the wake in the single-beam sonar system was determined based on the distribution of observation points in the ground truth bathymetric data. The direction is defined as the direction of the first principal component in $x - y$ space of the observation points. Pseudo-wakes were created at equal intervals in this direction. These were parallel to the wake direction, and the distances between the pseudo-wakes were set to a fixed distance. The pseudo-observation points were then set at equal intervals in the pseudo-wake. Finally, the data points closest to each pseudo-observation point were extracted from the ground truth bathymetric data.

In the experiment, the minimum number of pseudo-wakes in the sparse bathymetric data was three, the distance from other pseudo-wakes was 700 m, and the distance between the pseudo-observation points along the direction of the pseudo-wakes was 10 m.

#### 2) DENSE BATHYMETRIC DATA

Dense bathymetric data corresponding to sparse bathymetric data were also obtained from the ground truth data. First, a convex hull was computed for the points of sparse bathymetric data $P_{\mathrm{LR}}$, and the ground truth bathymetric data with observation points located within the convex hull were extracted. Subsequently, dense bathymetric data were created by sampling from the ground truth bathymetric data to $P_{\mathrm{LR}}$, such that these data did not overlap with the observation points. Figure 3 shows an example of sparse bathymetric data and the corresponding dense bathymetric data.

### D. POINT CLOUD UPSAMPLING MODEL

We adopted PU-GCN as a model for point cloud upsampling, we adopt PU-GCN [15]. This is a graph convolutional network based model, whose architecture is shown in Fig. 4. PU-GCN is a model with Inception DenseGCN as a feature extraction module and Nodeshuffle, which is based on PixelShuffle [21] proposed in image super-resolution, as a feature upsampling module. While PU-Net [12] and PU-GAN [14] perform upsampling by duplicating points in the latent space, PU-GCN enables upsampling using NodeShuffle, in which the GCN layer is integrated. The key feature of this model is that it can encode spatial information from the neighborhood of a point and learn new points from the latent space. The graph convolution used in the PU-GCN is EdgeConv, which was proposed in DGCNN [22].

## IV. EXPERIMENTS

The training dataset was created using the procedure described in Section III-B and–he PU-GCN was trained. The effectiveness of applying upsampling to sparse bathymetric data was analyzed.

### A. DATASET DETAILS

To evaluate the proposed method, 3571 target areas were divided into 70%, 10%, and 20% for training, validation, and evaluation, respectively. There is no overlap of sea areas in each dataset. The distribution of each divided area and sample at the mean depth are shown in Fig. 5 and 6, respectively. Multiple samples are available in the same area owing to the division of the sea area. To avoid an imbalance of samples in each area, a maximum of four samples were included in the dataset. Therefore, the numbers of point cloud samples used for training and evaluation were 5049 and 1352, respectively. In the training dataset, the number of points in all samples should be the same. Therefore, we sampled the same number of points in each sample constant using farthest point sampling.

In this experiment, the numbers of points for sparse bathymetric data $N$ and dense bathymetric data $rN$ were 1024 and 4096, respectively, as training data. The upsampling factor $r$ was set to four, following conventional studies on point cloud upsampling.

### B. IMPLEMENTATION DETAILS

During the training of the DNN model, normalization and data augmentation techniques were used to improve its generalization performance. For training a conventional point cloud upsampling model, the point cloud is normalized to fit a unit sphere, and methods such as rotation, translation, and scaling are used for data augmentation. However, these procedures are not directly applicable to the bathymetric data used in this study. In terms of normalization, the range of bathymetric values exhibited significant variation depending on the specific sea area from which the sample

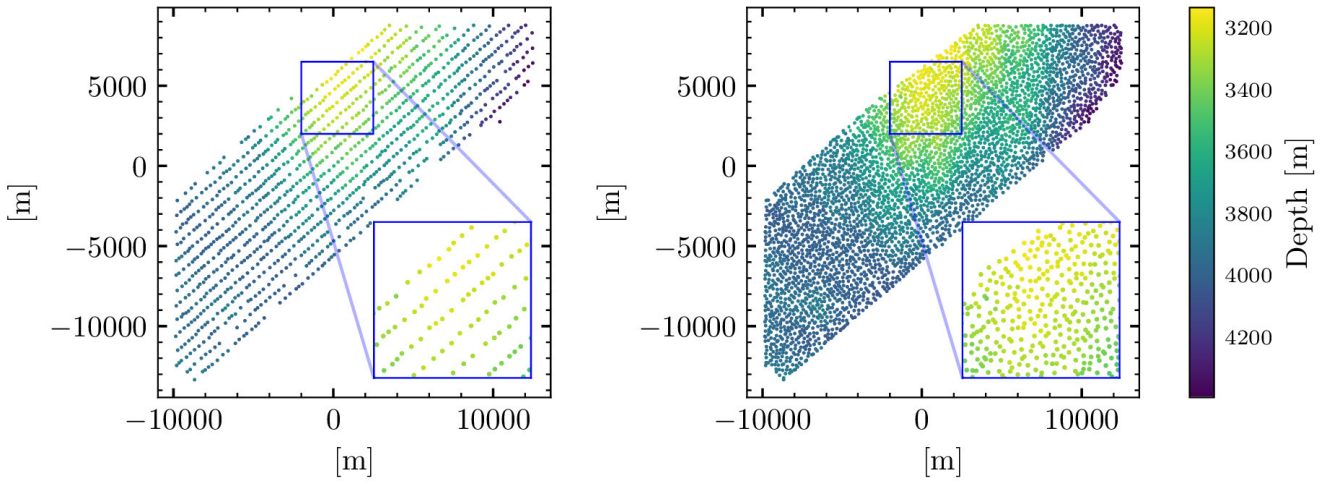


**FIGURE 3.** Sparse (left) and dense (right) bathymetric data. These are the bathymetric data pairs with an upscaling factor of 4. The sparse and dense bathymetric data are 1024 and 4096 points, respectively.

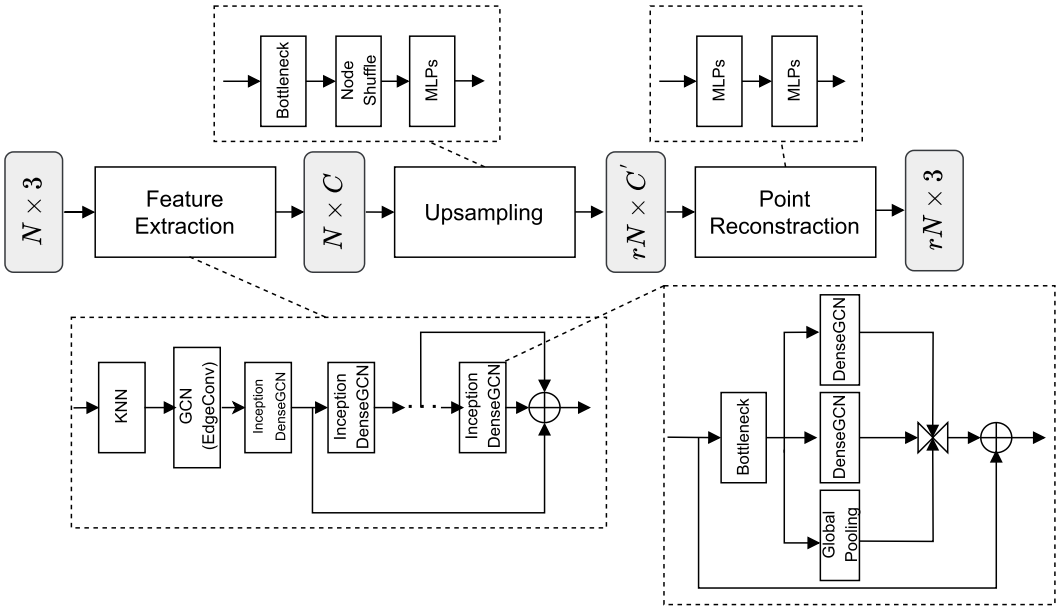


**FIGURE 4.** Architecture of PU-GCN [15]. Given an input point cloud, PU-GCN first constructs a graph using K-nearest neighbors, and then GCN embeds the 3D coordinates into latent space (feature extraction module). Subsequently, new points are generated by the upsampling module with Nodeshuffle (upsampling module) and reconstructed into 3D coordinates (point reconstraction module).

was derived. Therefore, each coordinate value was scaled by a constant factor for all the samples. In this experiment, the constant factor was set to $\frac{1}{7000}$ m. For data augmentation, the operations were limited to rotations about the $z$ axis and translation. Because the $x, y$ components are stripped of latitude and longitude information, bathymetric data are represented as seafloor topography and are invariant to the viewpoint.

The experiment was implemented using PyTorch, a deep-learning library. We used Adam [23] as the optimization function, with a learning rate of $1.0 \times 10^{-4}$. The batch size was 32, and the PU-GCN was trained using early stopping, which monitored the validation data to prevent overfitting (the maximum number of epochs was 300). The chamfer distance was used as the loss function. This measures the distance between the generated bathymetric data and the dense bathymetric data, which is the same as that in PU-GCN. This measures the distance between the generated bathymetric data $P$ and the dense bathymetric data $Q$ and follows the equation below:

$$d_{CD}(P, Q) = \frac{1}{|P|} \sum_{\boldsymbol{p} \in P} \min_{\boldsymbol{q} \in Q} \|\boldsymbol{p} - \boldsymbol{q}\|^2 + \frac{1}{|Q|} \sum_{\boldsymbol{q} \in Q} \min_{\boldsymbol{p} \in P} \|\boldsymbol{p} - \boldsymbol{q}\|^2$$

where $|P|$ and $|Q|$ are the number of points in $P$ and $Q$.

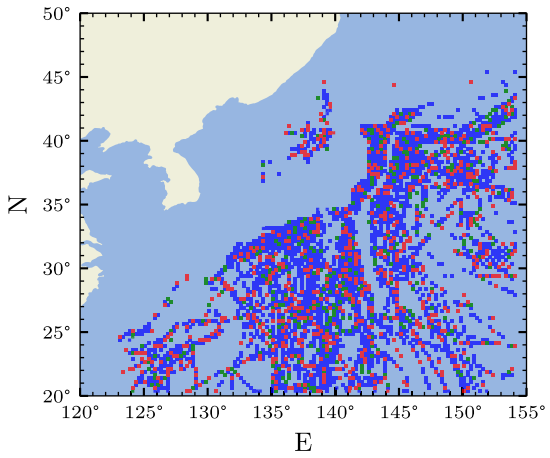


**FIGURE 5.** Sea areas used in this study. Blue, green, and red denote the sea area of training data, validation data, and evaluation data, respectively. Each grid represents a 15 arc-minutes, and there is no overlap in the training, validation, and evaluation data sets.

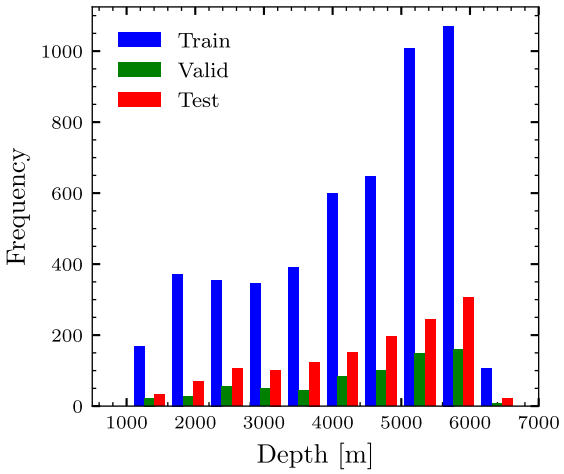


**FIGURE 6.** Frequency distribution at mean depth in the ground truth point cloud for each dataset. Blue, green, and red denote the sea area of training data, validation data, and evaluation data, respectively.

## V. EVALUATION

The point cloud upsampling model was evaluated by comparing the generated point cloud with the ground truth point cloud. Traditional evaluation metrics include the chamfer distance and the distance of the earth mover. However, this study focused on the ability to derive more detailed bathymetric maps by applying upsampling to sparse bathymetric data. Consequently, the upsampled point clouds were transformed into gridded data for evaluation. Specifically, a uniform grid size was established, and gridded data were constructed from each point cloud.

We used two methods to create gridded data from point clouds: Ordinary Kriging [6] and the K-nearest neighbor (KNN) method. In the experiment, the grid size was set to 200 m, and the number of neighbor points for the KNN method was set to 16.

### A. EVALUATION METRICS

The gridded data $D$ transformed from the point cloud were considered depth images, and the depth estimation task metric was used to evaluate the proposed method. Specifically, we evaluated the gridded data created from each point cloud using the five indices proposed in [24] and [25]. The following evaluation metrics were used:

$$\text{Abs-Rel} = \frac{1}{|D|}\sum_{z\in D}|\bar{z}-z|/\bar{z}$$

$$\text{Sq-Rel} = \frac{1}{|D|}\sum_{z\in D}\|\bar{z}-z\|^2/\bar{z}$$

$$\text{RMSE} = \sqrt{\frac{1}{|D|}\sum_{z\in D}\|\bar{z}-z\|^2}$$

$$\text{RMSE-Log} = \sqrt{\frac{1}{|D|}\sum_{z\in D}\|\log(\bar{z})-\log(z)\|^2}$$

$$\text{Threshold} : \%\ \text{of}\ z\ \text{s.t.}\ \max(\frac{\bar{z}}{z},\frac{z}{\bar{z}}) = \delta < thr$$

where $z$ is the bathymetric value of the grid and $\bar{z}$ is the ground truth value. In this experiment, $thr$ is set to 1.0025. Therefore, when the ground truth bathymetric value is 4000 m, the estimated value is correct if it is within $\pm 10$ m of the ground truth value.

### B. QUANTITATIVE RESULTS

Table 1 presents the results obtained using the evaluation metrics. The mean value was calculated based on 1352 evaluation data samples. For all indicators, the gridded bathymetric data generated using the proposed method exhibited better accuracy.

We further analyzed the effect of applying upsampling to sparse bathymetric data. Figure 7 shows the distribution of RMSE between the gridded bathymetric data generated from $P_{\text{LR}}$ and $P_{\text{SR}}$ and the ground truth gridded bathymetric data in the evaluation data.

Consequently, the gridded bathymetric data generated from the upsampled bathymetric data had a better RMSE for approximately 52% of the samples in the evaluation data. However, numerous samples with improved RMSE values are not distributed near the red line, and some have significantly improved RMSE. This means that a significant improvement in RMSE can be expected by applying upsampling. In fact, focusing on the samples with higher RMSE compared to the RMSE of the gridded bathymetric data generated from the $P_{\text{LR}}$, that is, samples located above the red line, the average difference in RMSE for each gridded bathymetric data was 2.07 m. However, for samples located below the red line, the difference was 9.56 m. Figure 8 shows the sea area of the evaluation data where the RMSE for the gridded bathymetric data improved or worsened by applying upsampling to the bathymetric data.

**TABLE 1. Results of quantitative evaluation by each gridded method GT type represents a method of converting from point clouds to gridded data. Bold type highlights the best performing models. *thr* is set to 1.0025.**

| GT Type | method | Abs-Rel↓ ($10^{-3}$) | Sq-Rel↓ ($10^{-3}$) | RMSE↓ (m) | RMSE-Log↓ ($10^{-3}$) | $\delta < thr \uparrow$ | $\delta < thr^2 \uparrow$ | $\delta < thr^3 \uparrow$ |
|---|---|---|---|---|---|---|---|---|
| Kriging | $P_{\mathrm{LR}}$ | 1.95 | 85.5 | 10.8 | 2.79 | 0.81 | 0.91 | 0.95 |
| | $P_{\mathrm{SR}}$ | **1.32** | **33.4** | **7.24** | **2.00** | **0.87** | **0.95** | **0.97** |
| KNN | $P_{\mathrm{LR}}$ | 1.56 | 35.4 | 9.56 | 2.55 | 0.83 | 0.93 | 0.96 |
| | $P_{\mathrm{SR}}$ | **1.30** | **22.3** | **7.82** | **2.11** | **0.87** | **0.95** | **0.98** |

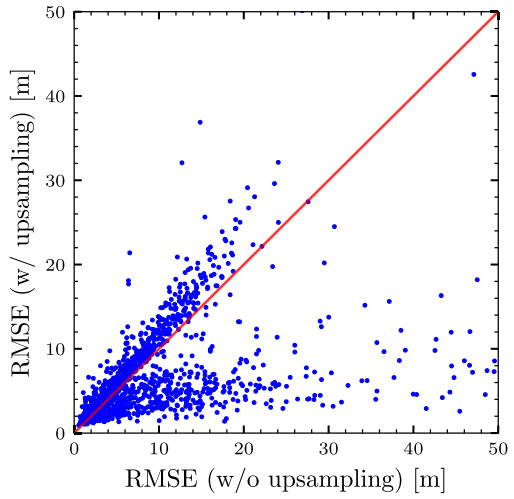


**FIGURE 7. Effect of upsampling on RMSE. Each point represents the RMSE for the gridded bathymetric data generated from $P_{\mathrm{LR}}$ and $P_{\mathrm{SR}}$. The red line indicates that there is no difference in RMSE before and after applying the proposed method. For the sake of the appearance of the graph, those with RMSEs of 50 m or more are considered outliers and are not plotted. The applicable samples were about 3% of the evaluation data.**

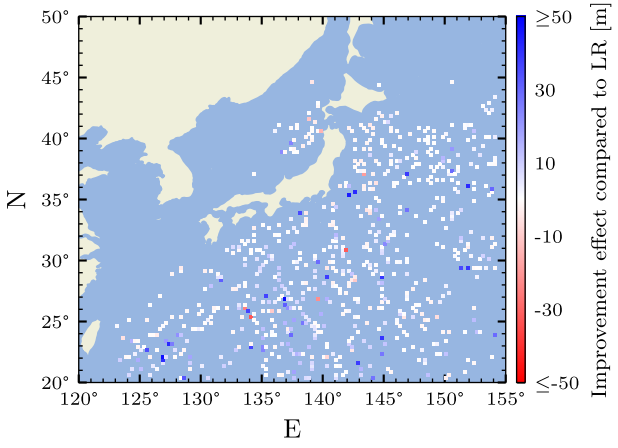


**FIGURE 8. Improved and worsened RMSE in sea areas by proposed method. Blue indicates areas where the RMSEs have improved, and red indicates areas where the RMSE have worsened. For sea areas with multiple samples, the average of each RMSE is calculated. For proper visualization, only the ocean areas where the difference in RMSE is in the range of ±50 m is plotted.**

We also analyzed the absolute bathymetric error in each grid of the gridded bathymetric data because the RMSE is affected by extreme values. In other words, we calculated the values for each grid for the bathymetric data as follows:

$$\Delta_{\mathrm{abs}} = |\bar{z} - z_{\mathrm{LR}}| - |\bar{z} - z_{\mathrm{SR}}|.$$

$z_{\mathrm{LR}}$ and $z_{\mathrm{SR}}$ denote the depths of the grid of gridded bathymetric data created from $P_{\mathrm{LR}}$ and $P_{\mathrm{SR}}$, respectively. If $\Delta_{\mathrm{abs}}$ is positive, the depth value of the target grid is closer to the true depth value obtained using the proposed method. We then calculated $\Delta_{\mathrm{abs}}$ for each grid of the gridded bathymetric data in the evaluation dataset and calculated the percentage (positive value) of the grid that was improved by applying upsampling to the entire grid. As shown in Fig. 7, the samples where the RMSEs are increased by the proposed method are not significantly different from the RMSEs of the gridded bathymetric data generated from the $P_{\mathrm{LR}}$. If the effect of the proposed method is small and negative, then it may not be problematic in certain contexts. Therefore, if $\Delta_{\mathrm{abs}}$ was negative for a grid and its value was within the acceptable range, we calculated the percentage improvement by applying upsampling which excluded that grid. Table 2 shows the percentage improvement achieved by applying upsampling when the allowed degradation range was varied by 2.0 m.

**TABLE 2. Improvement degree of upsampling in absolute bathymetric error.**

| Permissible distance (m) | 0.0 | 2.0 | 4.0 | 6.0 | 8.0 | 10.0 |
|---|---|---|---|---|---|---|
| Improved ratio (%) | 54 | 75 | 85 | 90 | 93 | 95 |

Consequently, if the permissible distance is 2.0 m, the proposed method can improve the absolute bathymetric error for 75% of the gridded bathymetric data.

### C. QUALITATIVE RESULTS

Figure 9 shows the samples with improved RMSE using the proposed method. The figure on the right side of each sample shows the $\Delta_{\mathrm{abs}}$ calculated for each grid. Gridded bathymetric data were generated using the Kriging method. The visual representation shows that the upsampled sample successfully reconstructed the topographic details of the ridges and valleys with increased accuracy. Conversely, Fig. 10 shows the gridded bathymetric data in cases where the proposed method produced negative effects. From this figure, the samples yielding less favorable results are characterized by relatively less complex and detailed topographic features in the ridges

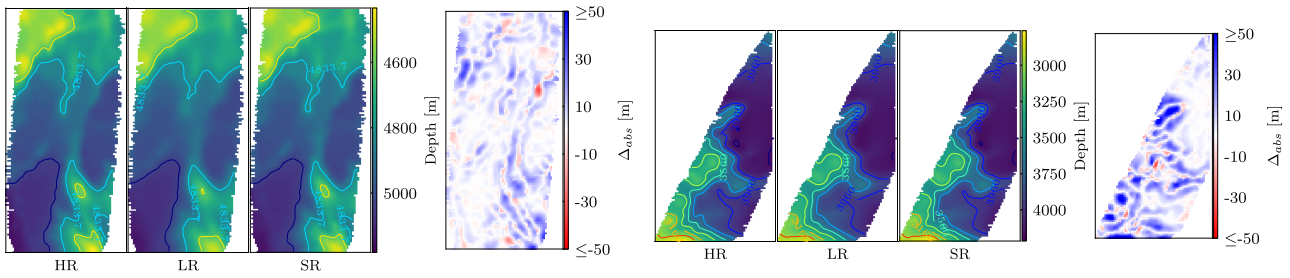


**FIGURE 9.** Examples of two samples with improved RMSE. We show samples with improved RMSE by applying the proposed method. From left to right, the gridded bathymetric data corresponding to the HR, LR, and SR point clouds are gridded, and $\Delta_{abs}$ is calculated for each grid. Grids with positive $\Delta_{abs}$ values represent an improvement in absolute depth error (blue), while grids with negative values represent a worsening of absolute depth error (red). We show in Fig.13 of the Appendix B each point cloud that was the source of these gridded bathymetric data.

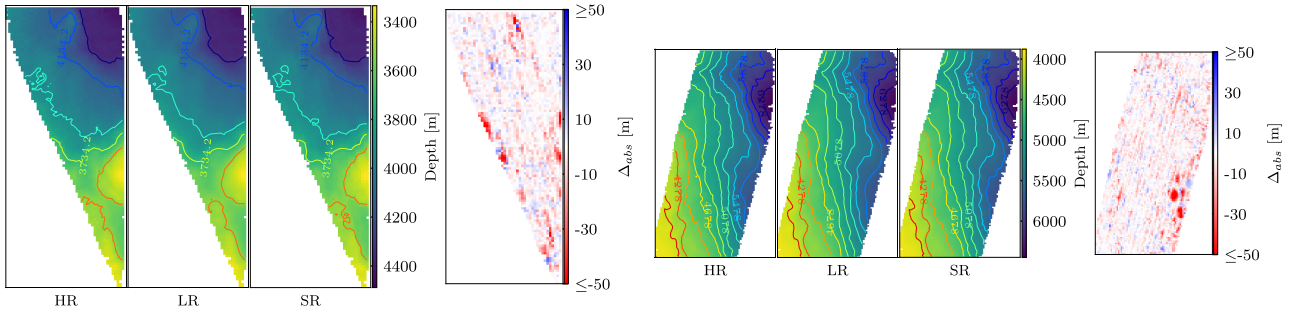


**FIGURE 10.** Examples of two samples with worse RMSE. In contrast to Fig. 9, we show figures for samples for which the RMSE worsened when our proposed method was applied.

and valleys. The input point cloud and upsampled point cloud before conversion to gridded data are shown in Fig. 13 of the Appendix B.

### D. QUANTITATIVE RESULTS EXCLUDING GRIDS CORRESPONDING TO SPARSE POINT CLOUDS

In the quantitative evaluation, the gridded bathymetric data generated from each point cloud were compared with the ground truth bathymetric gridded data. As the sparse point cloud, which is the input to the model, is created by thinning the ground truth point cloud, the grid corresponding to each point in the sparse point cloud is also the target of the evaluation calculations. To further validate the effectiveness of the proposed method, we performed a quantitative evaluation of each bathymetric grid dataset, excluding the grid corresponding to each point in $P_{\mathrm{LR}}$. The results are presented in Table 3. This shows that the proposed method captures detailed information on the seafloor topography.

### E. EVALUATION RESULTS FOR DIFFERENT DISTANCE BETWEEN PSEUDO-WAKES

We also created evaluation datasets with different distances between the pseudo-wakes for sparse bathymetric data. The distances between the pseudo-wakes were 800 m, 900 m, and 1000 m, and the direction of the pseudo-wakes for each sample was the same as that of the sample, with the distance between the pseudo-wakes set to 700 m. Figure 11 shows the results for the RMSE for each dataset. As shown in the figure, the RMSE of the gridded bathymetric data obtained by applying the proposed method decreased for all datasets.

## VI. DISCUSSION

In this study, we evaluated the effect of upsampling on bathymetric data and confirmed that more detailed bathymetric data could be obtained from sparse bathymetric data. This is the first attempt at point cloud upsampling for bathymetric data and will be the baseline method in this area.

Recently, studies have attempted to improve the quality of bathymetric data using multisource data fusion [26]. Our method can be applied to bathymetric data used in the aforementioned study, and higher-quality bathymetric data can potentially be obtained.

However, the proposed method has some limitations. First, the model generates new points based on the training data; however, the confidence level at these points is unknown. In the future, if the reliability of the generated points can be quantified, it will be feasible to use the model in various applications. Furthermore, as shown in Fig. 11, the effect of point cloud upsampling tended to decrease when the distance between pseudo-wakes of sparse bathymetric data increased. This indicates that it is difficult for the proposed model to generate detailed data when the input point cloud contains numerous blank areas. Therefore, we must verify the effectiveness of the modules of the current model and make

**TABLE 3.** Quantitative evaluation results for each grid method excluding grids corresponding to sparse point clouds Bold type describes the best performance. $LR_{grid}$ denotes the gridded data that contains each point in $P_{LR}$. *thr* is set to 1.0025.

| GT Type | method | Abs-Rel↓ ($10^{-3}$) | Sq-Rel↓ ($10^{-3}$) | RMSE↓ (m) | RMSE-Log↓ ($10^{-3}$) | $\delta < thr \uparrow$ | $\delta < thr^2 \uparrow$ | $\delta < thr^3 \uparrow$ |
|---|---|---|---|---|---|---|---|---|
| Kriging - $LR_{grid}$ | $P_{LR}$ | 2.06 | 88.8 | 11.3 | 2.94 | 0.80 | 0.90 | 0.94 |
| | $P_{SR}$ | **1.45** | **37.8** | **7.78** | **2.17** | **0.86** | **0.94** | **0.97** |
| KNN - $LR_{grid}$ | $P_{LR}$ | 1.75 | 43.1 | 10.4 | 2.81 | 0.81 | 0.92 | 0.96 |
| | $P_{SR}$ | **1.48** | **28.0** | **8.62** | **2.35** | **0.85** | **0.94** | **0.97** |

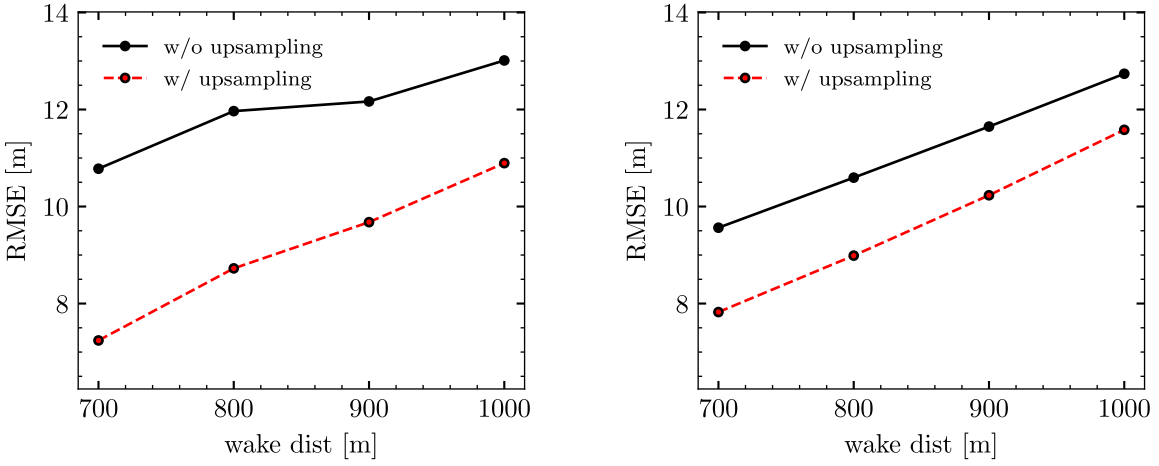


**(a)** Kriging method **(b)** KNN method

**FIGURE 11.** Quantitative results from Kriging and KNN methods The left figure shows the results from the Kriging method and the right figure from the KNN method. Solid line represents the average RMSE of the gridded bathymetric data generated from the $P_{LR}$ of each evaluation dataset. The dotted line represents that of the proposed method. The number of samples for the 700 m, 800 m, 900 m, and 1000 m datasets are 1352, 1351, 1349, and 1344, respectively. This is because the minimum number of pseudo-wakes is three.

improvements that are suitable for bathymetric data. These issues must be addressed in future studies.

## VII. CONCLUSION

We propose a method for obtaining detailed bathymetric data by applying a point cloud upsampling technique. To apply this technique, we created a dataset based on actual bathymetric data and trained a point cloud upsampling model. Qualitative and quantitative results indicate that increasing (upsampling) bathymetric data provides more detailed topographic information. The results showed that the improvement was more considerable when the seafloor topography was complex (that is, intricately interwoven ridges and valleys). As complex seafloor topography requires more point measurements than flat seafloor topography, the proposed method can be applied to efficiently understand bathymetry.

For producing high-quality bathymetric maps, a comparative analysis with grid-based bathymetric super-resolution is intriguing.

## APPENDIX A
## TRAINING PROCESS

To verify the reproducibility of the proposed method, the learning and validation losses in the learning process of the PU-GCN are shown in Fig. 12. The chamfer distance is used as the loss function.

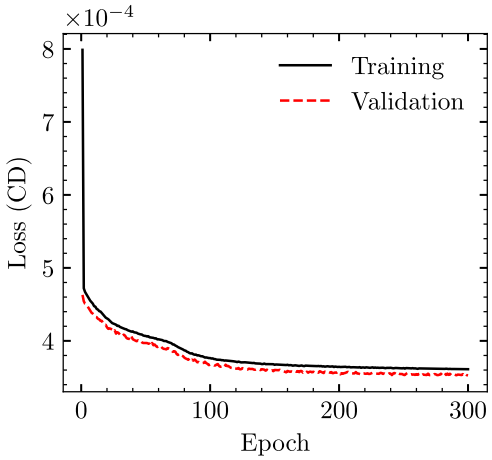


**FIGURE 12.** Training loss and validation loss for PU-GCN. The solid line represents the training data loss curve and the dotted line represents the validation data loss curve.

## APPENDIX B
## QUALITATIVE RESULTS OF POINT CLOUD UPSAMPLING

Figure 13 shows the point clouds that were the sources of each gridded bathymetric data point in Figs. 9, 10. Also

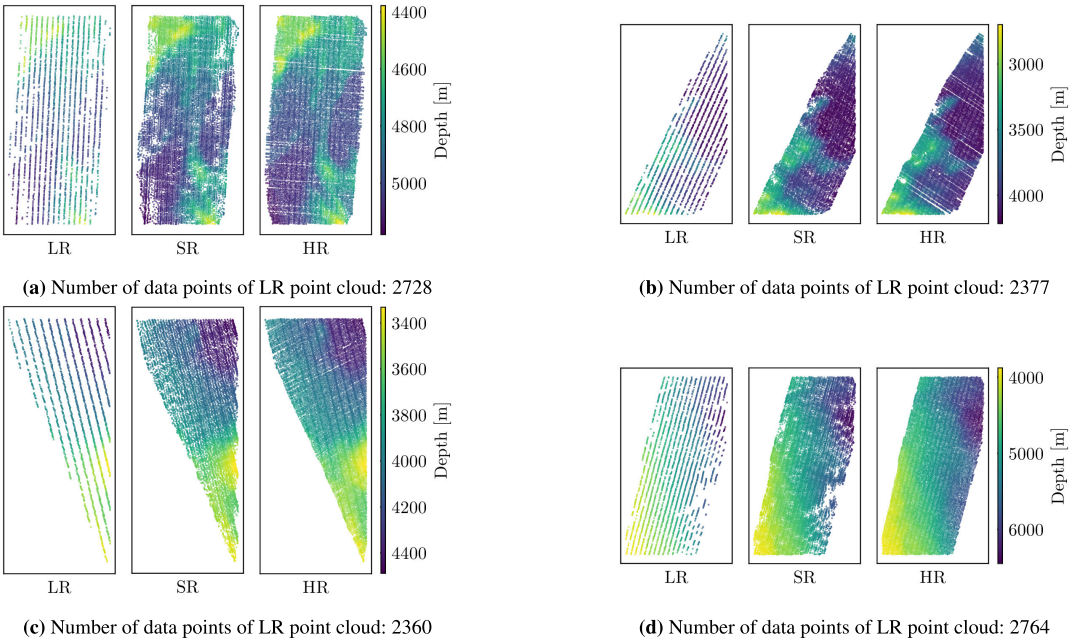


**(a)** Number of data points of LR point cloud: 2728

**(b)** Number of data points of LR point cloud: 2377

**(c)** Number of data points of LR point cloud: 2360

**(d)** Number of data points of LR point cloud: 2764

**FIGURE 13.** Each point cloud corresponding to the gridded bathymetric data. The upsampled point cloud (SR) shows that the data is close to high-resolution point cloud (HR). Please zoom in for more details.

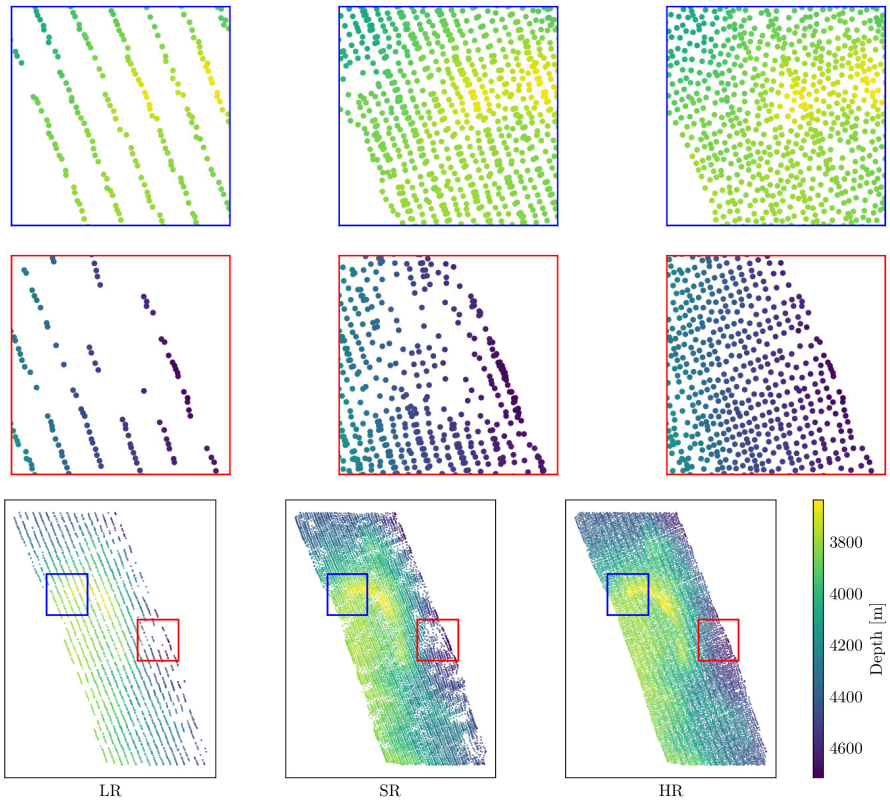


**FIGURE 14.** Upsampling quantitative results in bathymetric data. We show the input point cloud (2802 points), ×4 upsampled point cloud and high-resolution point cloud. Overall, the generated bathymetric data is similar to the true value.

shown in Fig. 14 is the data distribution for a sample with some of the areas zoomed in. The blue regions indicate that the proposed method produced data close to the true values. Conversely, the red regions are missing compared with the other regions, suggesting the need for additional observations. If the missing area of the observational data is large, the point cloud completion method may be more suitable than the upsampling method.

## REFERENCES

[1] T. H. Mohammadloo, M. Snellen, and D. G. Simons, "Assessing the performance of the multi-beam echo-sounder bathymetric uncertainty prediction model," *Appl. Sci.*, vol. 10, no. 13, p. 4671, Jul. 2020.
[2] Z. Li, Z. Peng, Z. Zhang, Y. Chu, C. Xu, S. Yao, Á. F. García-Fernández, X. Zhu, Y. Yue, A. Levers, J. Zhang, and J. Ma, "Exploring modern bathymetry: A comprehensive review of data acquisition devices, model accuracy, and interpolation techniques for enhanced underwater mapping," *Frontiers Mar. Sci.*, vol. 10, May 2023, Art. no. 1178845.
[3] *The Nippon Foundation-GEBCO Seabed 2030 Project*. Accessed: Aug. 19, 2023. [Online]. Available: https://seabed2030.org/
[4] M. Sonogashira, M. Shonai, and M. Iiyama, "High-resolution bathymetry by deep-learning-based image superresolution," *PLoS ONE*, vol. 15, no. 7, Jul. 2020, Art. no. e0235487.
[5] T. Yutani, O. Yono, T. Kuwatani, D. Matsuoka, J. Kaneko, M. Hidaka, T. Kasaya, Y. Kido, Y. Ishikawa, T. Ueki, and E. Kikawa, "Super-resolution and feature extraction for ocean bathymetric maps using sparse coding," *Sensors*, vol. 22, no. 9, p. 3198, Apr. 2022.
[6] J.-P. Chils, *Geostatistics: Modeling Spatial Uncertainty*. Hoboken, NJ, USA: Wiley, 2012.
[7] X. Wang, K. Yu, S. Wu, J. Gu, Y. Liu, C. Dong, Y. Qiao, and C. C. Loy, "ESRGAN: Enhanced super-resolution generative adversarial networks," in *Proc. Eur. Conf. Comput. Vis. (ECCV)*, Sep. 2018, pp. 63–79.
[8] B. Zhang, W. Xiong, M. Ma, M. Wang, D. Wang, X. Huang, L. Yu, Q. Zhang, H. Lu, D. Hong, F. Yu, Z. Wang, J. Wang, X. Li, P. Gong, and X. Huang, "Super-resolution reconstruction of a 3 arc-second global DEM dataset," *Sci. Bull.*, vol. 67, no. 24, pp. 2526–2530, Dec. 2022.
[9] B. Lim, S. Son, H. Kim, S. Nah, and K. M. Lee, "Enhanced deep residual networks for single image super-resolution," in *Proc. IEEE Conf. Comput. Vis. Pattern Recognit. Workshops (CVPRW)*, Jul. 2017, pp. 1132–1140.
[10] X. Li, J. Li, Z. Williams, X. Huang, M. Carroll, and J. Wang, "Enhanced deep learning super-resolution for bathymetry data," in *Proc. IEEE/ACM Int. Conf. Big Data Comput., Appl. Technol. (BDCAT)*, Dec. 2022, pp. 49–57.
[11] C. R. Qi, L. Yi, H. Su, and L. J. Guibas, "PointNet++: Deep hierarchical feature learning on point sets in a metric space," in *Proc. Adv. Neural Inf. Process. Syst.*, 2017, pp. 5099–5108.
[12] L. Yu, X. Li, C.-W. Fu, D. Cohen-Or, and P.-A. Heng, "PU-Net: Point cloud upsampling network," in *Proc. IEEE/CVF Conf. Comput. Vis. Pattern Recognit.*, Jun. 2018, pp. 2790–2799.
[13] H. Wu, J. Zhang, and K. Huang, "Point cloud super resolution with adversarial residual graph networks," 2019, *arXiv:1908.02111*.
[14] R. Li, X. Li, C.-W. Fu, D. Cohen-Or, and P.-A. Heng, "PU-GAN: A point cloud upsampling adversarial network," in *Proc. IEEE/CVF Int. Conf. Comput. Vis. (ICCV)*, Oct. 2019, pp. 7202–7211.
[15] G. Qian, A. Abualshour, G. Li, A. Thabet, and B. Ghanem, "PU-GCN: Point cloud upsampling using graph convolutional networks," in *Proc. IEEE/CVF Conf. Comput. Vis. Pattern Recognit. (CVPR)*, Jun. 2021, pp. 11678–11687.
[16] S. Qiu, S. Anwar, and N. Barnes, "Pu-transformer: Point cloud upsampling transformer," in *Proc. Asian Conf. Comput. Vis. (ACCV)*, Dec. 2022, pp. 2475–2493.
[17] R. J. G. B. Campello, D. Moulavi, and J. Sander, "Density-based clustering based on hierarchical density estimates," in *Advances in Knowledge Discovery and Data Mining*, J. Pei, V. S. Tseng, L. Cao, H. Motoda, and G. Xu, Eds. Berlin, Germany: Springer, 2013, pp. 160–172.
[18] J. Le Deunf, N. Debese, T. Schmitt, and R. Billot, "A review of data cleaning approaches in a hydrographic framework with a focus on bathymetric multibeam echosounder datasets," *Geosciences*, vol. 10, no. 7, p. 254, Jul. 2020.
[19] H. Bisquay, X. Freulon, C. De Fouquet, and C. Lajaunie, "Multibeam data cleaning for hydrography using geostatistics," in *Proc. OCEANS*, Sep. 1998, pp. 1135–1143.
[20] J. Long, H. Zhang, and J. Zhao, "A comprehensive deep learning-based outlier removal method for multibeam bathymetric point cloud," *IEEE Trans. Geosci. Remote Sens.*, vol. 61, 2023, Art. no. 4201622.
[21] W. Shi, J. Caballero, F. Huszár, J. Totz, A. P. Aitken, R. Bishop, D. Rueckert, and Z. Wang, "Real-time single image and video super-resolution using an efficient sub-pixel convolutional neural network," in *Proc. IEEE Conf. Comput. Vis. Pattern Recognit. (CVPR)*, Jun. 2016, pp. 1874–1883.
[22] Y. Wang, Y. Sun, Z. Liu, S. E. Sarma, M. M. Bronstein, and J. M. Solomon, "Dynamic graph CNN for learning on point clouds," *ACM Trans. Graph.*, vol. 38, no. 5, pp. 1–12, Oct. 2019.
[23] D. P. Kingma and J. Ba, "Adam: A method for stochastic optimization," 2014, *arXiv:1412.6980*.
[24] D. Eigen, C. Puhrsch, and R. Fergus, "Depth map prediction from a single image using a multi-scale deep network," in *Proc. Adv. Neural Inf. Process. Syst.*, 2014, pp. 2366–2374.
[25] L. Ladický, J. Shi, and M. Pollefeys, "Pulling things out of perspective," in *Proc. IEEE Conf. Comput. Vis. Pattern Recognit.*, Jun. 2014, pp. 89–96.
[26] U. Lebrec, V. Paumard, M. J. O'Leary, and S. C. Lang, "Towards a regional high-resolution bathymetry of the North West Shelf of Australia based on Sentinel-2 satellite images, 3D seismic surveys, and historical datasets," *Earth Syst. Sci. Data*, vol. 13, no. 11, pp. 5191–5212, Nov. 2021.

**NAOYA IRISAWA** received the B.S. and M.S. degrees in mathematics from Hokkaido University, Sapporo, Japan, in 2019 and 2021, respectively. He is currently pursuing the Ph.D. degree with the Graduate School of Data Science, Shiga University, Hikone, Japan. His research interests include point cloud upsampling, super-resolution, image inpainting, and machine learning.

**MASAAKI IIYAMA** (Member, IEEE) received the B.S. degree in engineering informatics and the M.S. and Ph.D. degrees in informatics from Kyoto University, in 1998, 2000, and 2006, respectively. He was a Research Associate and an Assistant Professor with Kyoto University, from 2003 to 2006 and from 2006 to 2015, respectively. He is currently a Professor with the Faculty of Data Science, Shiga University. His research interests include image processing, computer vision, and remote sensing.